2A.2

EXPERIMENTAL FORECASTS OF MOUNTAIN WAVES FOR THE TERRAIN-INDUCED ROTOR EXPERIMENT (T-REX)

Ligia Bernardet[1, 2], Brian Jamison[1,3], John Brown[1], Steven Koch[1], and Jimy Dudhia[4]

[1]NOAA Earth System Research Laboratory, Boulder, CO
[2]Systems Research Group, Inc., Colorado Springs, CO
[3]Cooperative Institute for Research in Environmental Studies, University of Colorado, Boulder, CO
[4]National Center for Atmospheric Research, Boulder, CO

1. INTRODUCTION

The main objective of the Terrain-Induced Rotor Experiment (T-REX) is to understand the nature of the coupling of mountain-induced rotor circulations to the structure and evolution of overlying mountain waves and to the underlying boundary layer (Grubisic et al. 2004). T-REX results also aim at increasing the understanding of mountain wave dynamics, including their generation, propagation, and breakdown. The field phase of T-REX took place in March and April 2006 in the Owens Valley region, directly east of the southern Sierra Nevada, the tallest quasi-two-dimensional mountain range in the conterminous US. The eastern escarpment from the crest of the southern Sierra to the Owens Valley consists of a drop in elevation of 3km in a distance of approximately 10km.

Several groups ran high-resolution non-hydrostatic models in support of either the real-time or research objectives of T-REX. Of particular interest is the ability of the Weather Research and Forecasting (WRF) model to correctly predict mountain waves. The WRF model was developed to serve both research and operational needs. It currently supports two dynamic cores: the Advanced Research WRF (ARW) core developed at NCAR (Skamarock et al. 2005) and the Non-hydrostatic Mesoscale Model (NMM) core, developed at NCEP (Janjic et al. 2001). The WRF model is currently running in several applications at the National Centers for Environmental Prediction (NCEP):

- The North-American Mesoscale Model (NAM) employs the NMM core of WRF, in a domain that covers all of North America with a grid spacing of 12 km.
- The Short-Range Ensemble Forecast (SREF) has both NMM and ARW members, with a domain that covers much of North America and adjacent portions of the Pacific Ocean with a grid spacing of 32 km.
- The Hurricane WRF employs the NMM core.
- The High-Resolution Window (HRW) WRF has both NMM and ARW cores running with grid spacings of 5.1 and 5.8 km, respectively. Several regional domains are run: eastern CONUS, central CONUS, western CONUS, Puerto Rico, Alaska, and Hawaii.

The ARW and NMM cores of WRF differ in a variety of aspects, such as: map-projection, grid-staggering, vertical coordinate, numerical solver, diffusion, divergence damper, and top boundary condition. It is worth noting that, while the NMM has no special treatment of diffusion near the top boundary, the ARW was configured with a 5-km deep layer near the top boundary where extra diffusion was added to reduce wave reflection.

The objectives of this study are to compare and contrast the ARW and NMM forecasts, and to compare those forecasts against in-situ aircraft observations collected during the field phase of T-REX. Two Intensive Observation Periods (IOPs) were chosen for this comparison: IOP 10 and IOP 13, in which weak and strong mountain waves were observed, respectively. The observational datasets used in this study are in-situ observations taken by the National Science Foundation High-performance Instrumented Airborne Platform for Environmental Research (HIAPER) aircraft and by the United Kingdom Natural Environmental Research Council UK BAe146 aircraft, which is jointly managed the UK Met Office and the consortium of UK universities.

2. MODEL CONFIGURATION

Given the importance of correctly forecasting mountain waves, which can be associated with rotors that are extremely hazardous to aviation, and the

* *Corresponding author address:* Ligia Bernardet NOAA ESRL R/GSD7 325 Broadway Boulder, CO 80305 E-mail: ligia.bernardet@noaa.gov.

generalized use of the WRF model in operations, it is important to evaluate the WRF model's ability to forecast mountain waves. To this end, the National Oceanic and Atmospheric Administration (NOAA) Earth System Research Laboratory (ESRL) and the WRF Developmental Testbed Center (DTC) joined efforts to run the ARW and NMM cores of the WRF model daily during the field phase of T-REX (Koch et al 2006). Both cores were configured with very high-resolution: 2-km grid spacing, over a square 450 km on each side over the T-REX region of study (Fig. 1). Both cores were run with 50 vertical levels, with the model top at 50 hPa. The cores were initialized using the WRF Standard Initialization (SI) from the Rapid Update Cycle (RUC) analysis and used the North American Mesoscale Model (NAM - Eta model) forecasts for boundary conditions. Forecasts were initialized at 00 and 12 UTC and run out to 24 h. It should be pointed out that due to the lack of observations over the Pacific Ocean, there is large uncertainty in the initial state of the model, which impacts the confidence in the resulting forecasts.

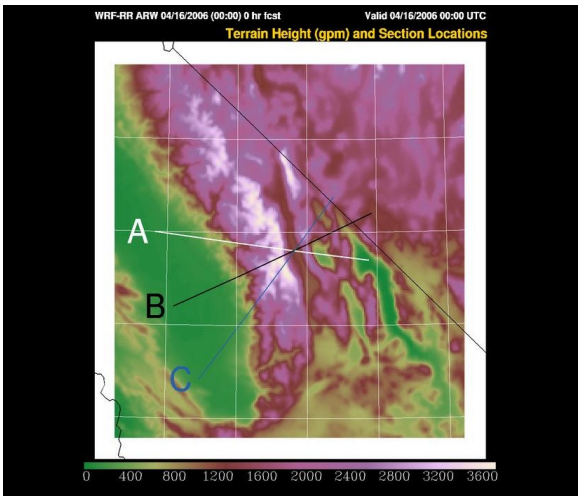

Figure 1. Forecast domain, showing topographical height (m) and the location of cross-section B. The thin black line stretching in the NW-SE direction is the border between California and Nevada.

To allow for a controlled comparison, the ARW and NMM were configured as similarly as possible, so that the differences were limited to dynamic core. Version 2.1.2 of the WRF model code was modified so that the NAM physics suite (Table 1) could run on both cores (Benjamin and Brown 2006). This code was originally developed for the Rapid Refresh Core Test (Nance 2006) to support the implementation of the Rapid Refresh WRF at NCEP.

Table 1. Physical parameterizations used in the ARW and NMM runs.

Microphysics	Ferrier
Convection	None
Radiation	GFDL
Surface Layer	Janjic
Planetary Boundary Layer	Mellor-Yamada-Janjic
Land Surface Model	Noah

3. IOP-10

This IOP featured a moderate amplitude trapped mountain wave event. The mountain wave activity was associated with a long-wave trough that was oriented such that a 40-knot southwesterly flow was impinging on the Sierra at 500 hPa. The flow at 700 hPa was considerably weaker with a 15-20 knot upstream flow. A shortwave trough moved through the long-wave trough and provided a period of enhanced westerly flow just prior to 12UTC 8 April.

To take advantage of a time period in which both HIAPER and BAe146 observations are available, comparisons between model and observations will be presented using the model initialized at 00 UTC on April 08, 2006 valid at 18 UTC on April 08.

Both forecasts depict strong upward motion on the upper portion of the western slope of the Owens Valley, with higher intensity found in the ARW (Fig. 2 shows results along Cross-section B - see Fig. 1 for the location of this cross-section). The ARW shows strong downward motion on the western slope of the Valley, which is not seen in the NMM. The ARW has a quiescent structure upstream and downstream from the steepest topography, while the NMM has several waves in both directions. The ARW also shows more wave activity in the lower stratosphere.

The HIAPER flew this mission at a height of approximately 11.3 km. Fig. 3 indicates that there was more wave activity in the observations than in the forecasts. The HIAPER identified vertical velocities from -1.4 to +1.4 m s^{-1}, with 5 waves with wavelength of 15 km. The ARW captured fairly well the amplitude, wavelength and placement of the first two waves, but missed the location and intensity of the other waves. The NMM vertical velocities only reached between -0.5 and +1.0 m s^{-1}, and the phase of the waves does not match the observations. The comparison between observed and forecasted potential temperature (Fig. 4) indicates a bias, with

the forecasts generally presenting lower potential temperature than the observations, indicating a possible displacement in the forecasted tropopause location. As with the vertical velocity, the ARW represents well the location and wavelength of the westernmost waves but missed the others.

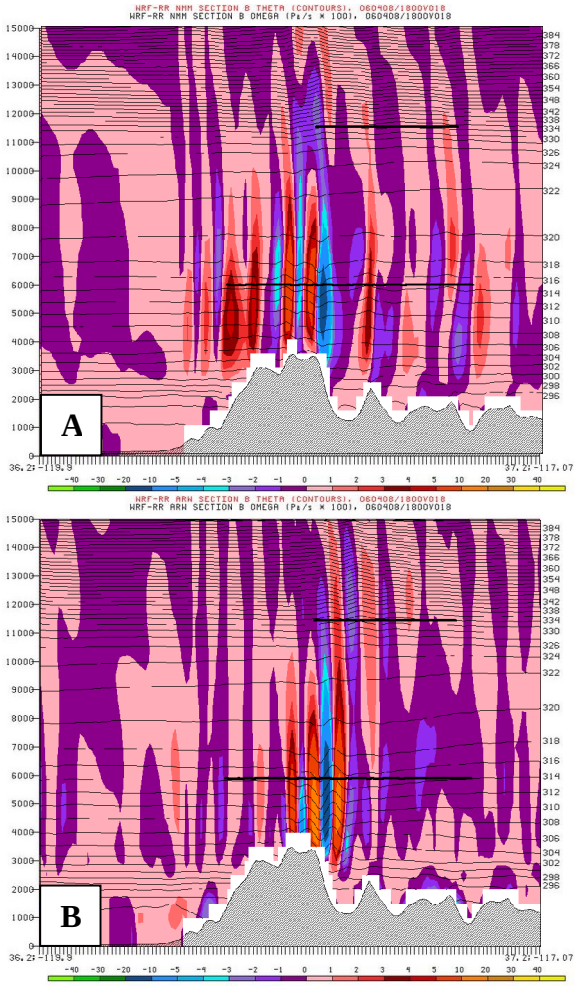

Figure 2. Eighteen hour forecast of pressure vertical velocity (Pa/s x 100) along cross-section B valid at 18 UTC on April 08, 2006 for the a) NMM and b) ARW. The HIAPER and Bae146 flight legs are shown as thick black lines heights of approximately 11.3 and 6.0 km, respectively.

Fig. 5 depicts a comparison between the BAe146 observations and the ARW and NMM forecasts at a height of approximately 6 km. The observations show several local maxima of vertical velocity, with an absolute maximum of 1.7 m s^{-1} 58 km into the flight. This maximum is flanked on both sides by downdrafts between -1 and -2 m s^{-1}. Both cores overestimated the maximum in vertical velocity, with the ARW reaching up to 3.2 m s^{-1}. With respect to the flanking downdrafts, both cores represent the western downdraft, with the ARW capturing well its magnitude and the NMM underestimating it. The eastern downdraft is only represented in the ARW, with the NMM actually displaying upward motion. Downstream from the main wave, the observations show vertical velocities oscillating between +- 1 m/s, while the models have much smaller values.

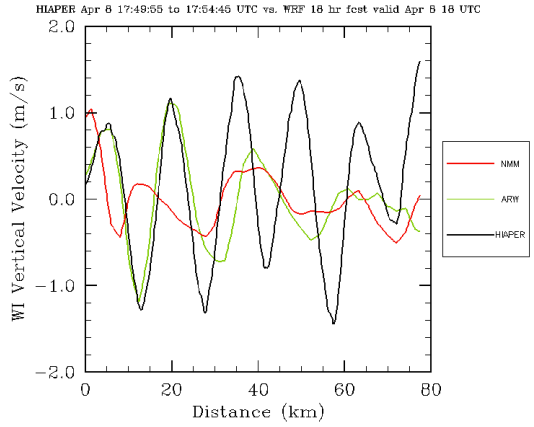

Figure 3. Vertical velocity (m s^{-1}). from observations (black) and forecasts along the HIAPER flight segment on Cross-section B. The NMM (red) and ARW (green) were initialized at 00 UTC of April 08, 2006 and are valid at 18 UTC of April 08, 2006.

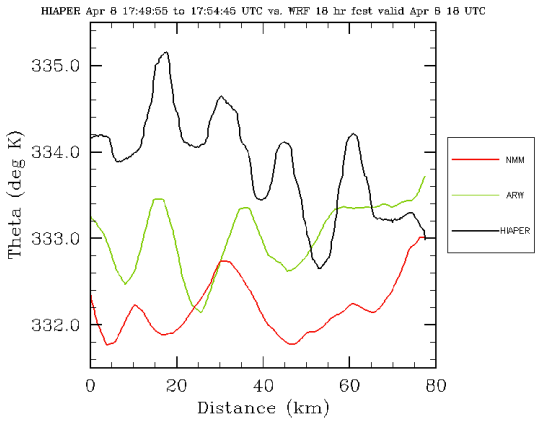

Figure 4. Same as Fig.3, except for potential temperature (K).

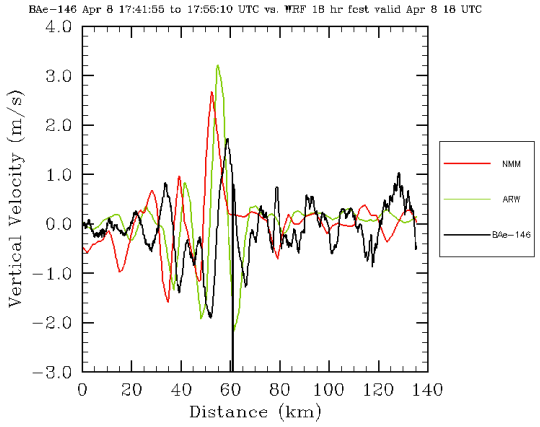

Figure 5. Same as Fig. 3, but for the BAe146 aircraft instead of the HIAPER.

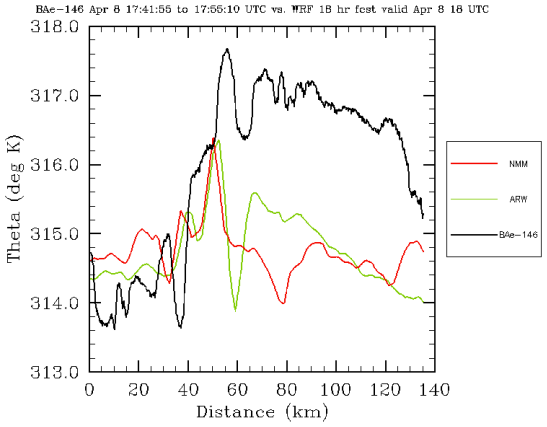

Figure 6. Same as Fig. 5, but for potential temperature (K).

The potential temperature comparison (Fig. 6) indicates that the forecasts are more similar to each other than to the observations. Differences with the observations are particularly remarkable in the eastern half of the flight leg, where the forecasted potential temperatures are about 2 K lower than the observed ones. The positive potential temperature perturbation associated with the strongest vertical velocity is of the same magnitude in the observations and forecasts, around 1.0 K. Beyond that, the correspondence between forecasts and observations is not straightforward.

4. IOP-13

One of the strongest mountain wave and rotor events of the experiment occurred during this IOP. The large-scale scenario for this event included a 500 hPa amplifying trough with strong westerly winds at 700 hPa. This led to the development of a strong downslope windstorm in the lee of the Sierra Mountain and well developed vertically propagating gravity waves.

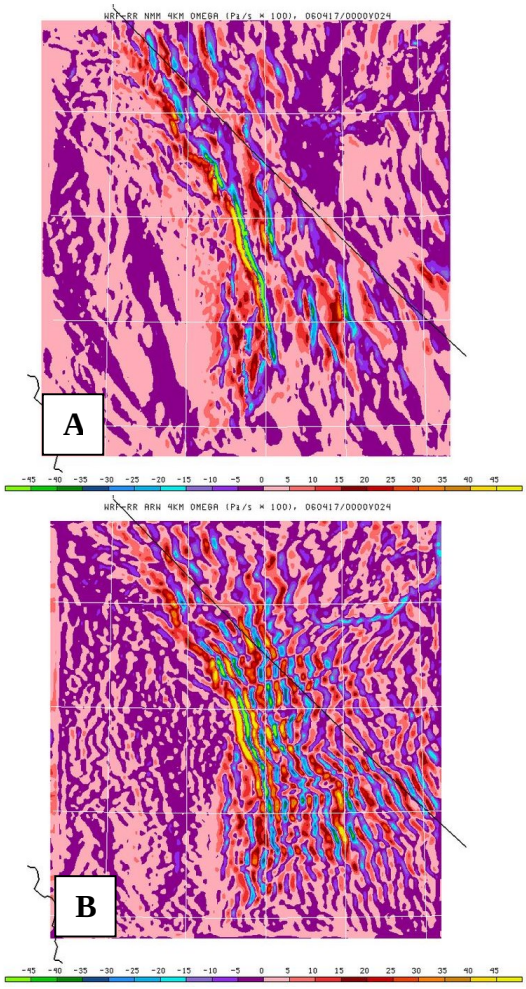

Figure 7. Twenty-four hour forecast of 4 km MSL pressure vertical velocity (Pa/s x 100) valid at 00 UTC on April 17, 2006 for the a) NMM and b) ARW.

For this IOP, this study focuses on the forecast initialized at 00 UTC of April 16, 2006. The 24-h forecast of 4km MSL pressure vertical velocity (Fig.

7) shows significant differences between the ARW and NMM forecasts. While the maximum vertical velocities are similar for both cores, the NMM shows one strong wave at the western end of the Owens Valley, and a secondary wave at the eastern end of the Valley. In contrast, the ARW produced an organized train of waves over a broad region to the lee of the Sierras. Additionally, everywhere in the domain, the ARW generated more small-scale structures than the NMM.

At 10 km MSL, Fig. 8 shows that the NMM produced stronger vertical velocities concentrated over a narrow band parallel to the topographical barrier. Consistently with the forecasts at 4-km MSL, the ARW produced a more organized train of waves to the lee of the Inyo Mountains.

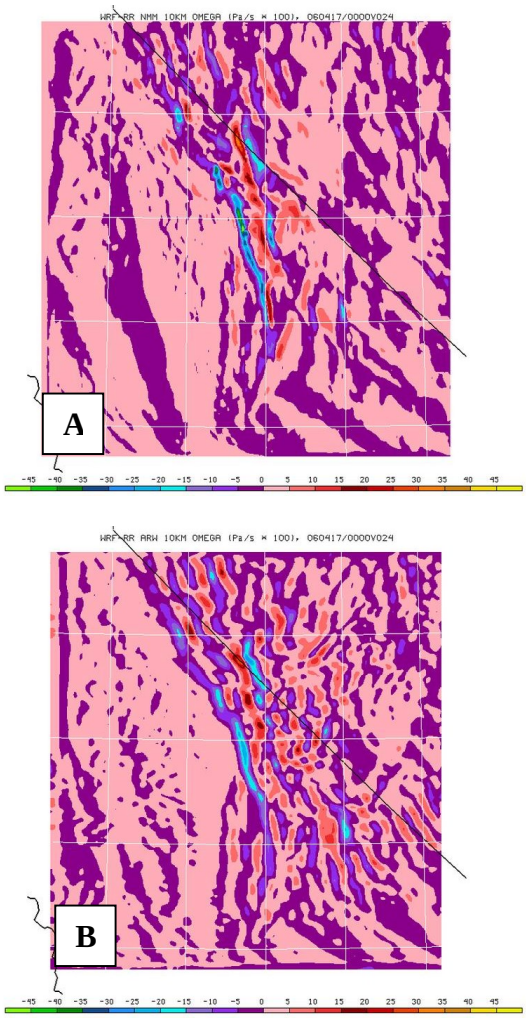

Figure 8. Same as Fig 7., except for 10 km MSL.

The 24-h forecast of pressure vertical velocity is shown in Fig. 9 for Cross-section B. The path of the HIAPER flight is depicted as a thick black line at an approximate height of 9.3 km.

Both cores depict strong downward motion over the crest of the Sierras, associated with strong upward motion just downstream, with the ARW bringing the downward motion farther into the valley. Both models also depict downward motion along the eastern slope of the Valley, followed by a train of waves, which is more coherent in the ARW.

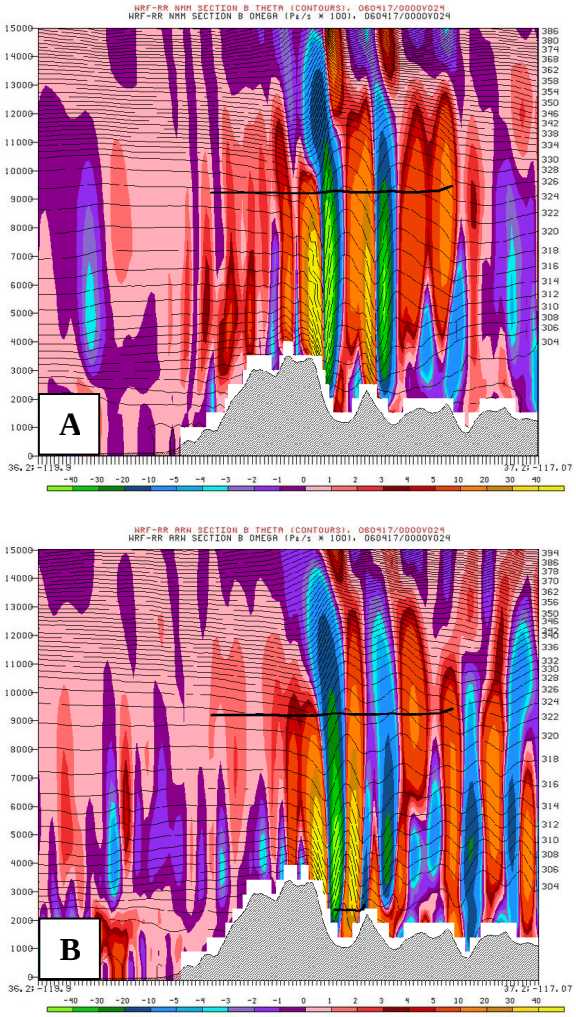

Figure 9. Twenty-four hour forecast of pressure vertical velocity (Pa/s x 100) along cross-section B valid at 00 UTC on April 17, 2006 for the a) NMM and b) ARW. The HIAPER flight leg is shown as a thick black line at a height of approximately 9.3 km.

The comparison with the HIAPER shows that the models exaggerate the magnitude of the wave on the western slope of the Owens Valley: while the potential temperature perturbation in the observations is only about 1 K, it exceeds 2 K in the NMM and 4 K in the ARW (Fig. 10). The observations show a stronger perturbation along the eastern slope of the valley. This wave is well captured by the NMM, while the ARW forecast is too weak.

The vertical velocity observations (Fig. 11) show two complete waves, with maxima at 3 and 6 m s^{-1} and the minima at –7 and –4 m s^{-1}. As with the potential temperature, both cores exaggerate the first wave maximum. The NMM captures well the location and magnitude of the first minimum and the second maximum, while the ARW underestimates both, and places the downward motion displaced to the west. Both models forecast the second minimum in vertical velocity, even though the magnitude is slightly underestimated and the ARW has a phase displacement to the west. The observations show a smaller vertical velocity peak on the end of the flight leg, which has too small magnitude and is displaced to the west in both cores.

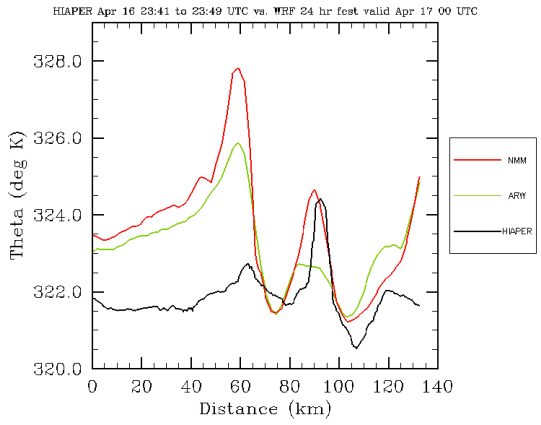

Figure 10. Potential temperature (K) from observations (black) and forecasts along the HIAPER flight segment on Cross-section B. The NMM (red) and ARW (green) were initialized at 00 UTC of April 16, 2006 and are valid at 24 UTC of April 17, 2006.

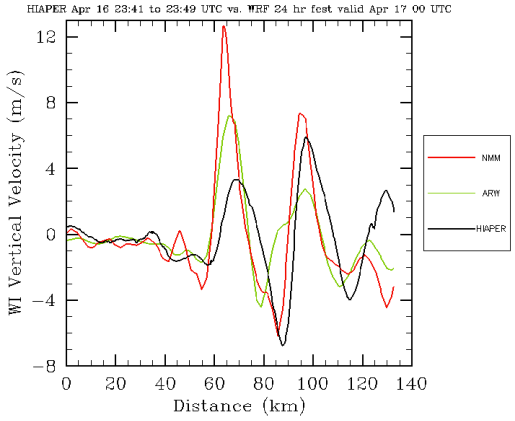

Figure 11. Same as Fig. 10, except for vertical velocity (m s^{-1}).

5. CONCLUSIONS

The ARW and NMM cores of the WRF model were contrasted and compared against observations for two IOPs of T-REX. The cases were selected to represent the development of weak (IOP-10) and strong (IOP-13) mountain waves. The HIAPER and BAe146 aircraft in-situ observations were used to verify the forecasts.

The results showed that, in IOP-10, the ARW produced mountain waves with stronger vertical motion and greater propagation to upper levels than the NMM. The observations support the larger wave activity seen in the ARW. The ARW also captured well the downward motion above the western slope of the Owens Valley. Conversely, in IOP-13, the NMM produced more intense vertical motion than the ARW. For IOP 13, both cores exaggerated the maximum vertical velocity at the 9.3-km level in which comparisons with observations were carried. A significant difference between the forecasts produced with both cores was a tendency of the ARW in producing organized trains of waves downstream from the steepest topography. The reasons for these differences, which could be related to the top boundary conditions, the vertical coordinates, the divergence dampers, or other aspects of the numeric schemes, are currently being investigated.

These preliminary conclusions indicate that the two cores of the WRF model can produce significantly different forecasts of mountain waves. This result adds to the Rapid Refresh Core Test (Nance 2006, Benjamin and Brown 2006) to support the implementation of the Rapid Refresh WRF at NCEP. For that test, conducted at 13 km grid spacing, small differences were encountered between the forecast verification statistics obtained from the two cores. Therefore, it is recommended that additional dynamic core tests be conducted at higher resolutions in order to highlight differences in the results.

6. REFERENCES

Benjamin, S. and J. Brown, 2006: WRF Rapid Refresh dynamic Core evaluation and recommendation. Available at http://ruc.fsl.noaa.gov/coretest2/WRF_Rapid_Refresh_dynamic_core_recommendation-31aug06.pdf

Grubisic, V., J. Doyle, J. Kuettner, G. S. Poulos, and C. D. Whiteman, 2004: T-REX: Terrain-Induced Rotor Experiment overview document and experimental design. 72 pp. Available at http://www.eol.ucar.edu/projects/trex/documents/TREX_SOD.pdf.

Janjic, Z. I., J. P. Gerrity, Jr. and S. Nickovic, 2001: An Alternative Approach to Nonhydrostatic Modeling. *Mon. Wea. Rev.*, **129**, 1164-1178.

Koch, S., L. Bernardet, B. Jamison, and J. Brown, 2006: Modeling of mountain waves in T-REX. *12th Conf. on Mountain Meteorology*, Amer. Meteor. Soc. Available at http://ams.confex.com/ams/pdfpapers/114583.pdf].

Nance, L., 2006: Weather Research and Forecasting Core Test: WRF DTC Report. [Available from Developmental Testbed Center, NCAR, P.O. Box 3000, Boulder, CO, 80307-3000 or online at http://ruc.fsl.noaa.gov/coretest2/DTC_report.pdf.]

Skamarock, W. C., J. B. Klemp, J. Dudhia, D. O. Gill, D. M. Barker, W. Wang, and J. G. Powers, 2005: A description of the Advanced Research WRF Version 2. NCAR Technical Note 468+STR, 88 pp.